PHYSICS

Experimental entanglement of 25 individually accessible atomic quantum interfaces

Yunfei Pu,[1] Yukai Wu,[1,2] Nan Jiang,[1] Wei Chang,[1] Chang Li,[1] Sheng Zhang,[1] Luming Duan[1,2]*

A quantum interface links the stationary qubits in a quantum memory with flying photonic qubits in optical transmission channels and constitutes a critical element for the future quantum internet. Entanglement of quantum interfaces is an important step for the realization of quantum networks. Through heralded detection of photon interference, we generate multipartite entanglement between 25 (or 9) individually addressable quantum interfaces in a multiplexed atomic quantum memory array and confirm genuine 22-partite (or 9-partite) entanglement. This experimental entanglement of a record-high number of individually addressable quantum interfaces makes an important step toward the realization of quantum networks, long-distance quantum communication, and multipartite quantum information processing.

INTRODUCTION

Stationary qubits carried by the ground states of cold atoms are an ideal memory for storage of quantum information, whereas flying photonic pulses are the best choice for the transmission of quantum information through the optical communication channels. A quantum interface can convert the stationary qubits into flying photonic pulses and vice versa and therefore generates an efficient link between the quantum memory and the optical communication channels (*1*). A good quantum memory is provided by the hyperfine states of single atoms (ions) or the collective states of an atomic ensemble. Compared with single atoms or ions, the collective state of an atomic ensemble cannot be easily controlled for performing qubit rotations and qubit-qubit gate operations, and therefore it is not a convenient qubit for the realization of quantum computation. However, because of the collective enhancement effect, the collective state of an optically dense atomic ensemble has a unique advantage of strong coupling to the directional emission even in the free space, which generates an efficient quantum link between the atomic memory and the forward-propagating photonic pulses and hence provides an ideal candidate for the realization of the quantum interface (*1*–*3*). For the implementation of quantum networks, long-distance quantum communication, and the future quantum internet, a promising way of scaling up is based on generating entanglement between these efficient quantum interfaces (*1*–*6*). Remarkable experimental advances have been reported toward this goal (*7*–*17*). As the state of the art, up to four atomic ensemble quantum interfaces have been entangled through the heralded photon detection (*14*).

Here, we report a significant advance in this direction by experimentally generating multipartite entanglement between 25, 16, and 9 individually addressable atomic quantum interfaces and confirm genuine 22-, 14-, and 9-partite entanglement, respectively, for these cases with a high confidence level by measuring the entanglement witness. Through programmable control and heralded detection of photon interference from a two-dimensional (2D) array of micro atomic ensembles, we generate and experimentally confirm the multipartite W-state entanglement, which is one of the most robust types of many-body entanglement and has applications in various quantum information protocols (*18*–*22*). Tens to thousands of atoms in a single atomic ensemble have been entangled with heralded photon detection (*21*, *22*). However, in those cases, the atoms are not separable or individually addressable, and we do not have multipartite entanglement between individual quantum interfaces. In other experimental systems, up to 14 ions (*23*), 10 photons (*24*), and 10 superconducting qubits (*25*) have been prepared into genuinely entangled states. Those experiments generate multipartite entanglement between individual particles, but each particle alone cannot act as an efficient quantum interface to couple the memory qubits with the flying photons. Our experiment achieves multipartite entanglement between a record-high number of individually addressable quantum interfaces and demonstrates an important enabling step toward the realization of quantum networks, long-distance quantum communication, and multipartite quantum information processing (*1*–*6*, *18*, *19*).

RESULTS

Experimental setup

Our experimental setup is illustrated in Fig. 1. We divide a macroscopic ^{87}Rb atomic ensemble into a 2D array of micro-ensembles (*26*). Each micro-ensemble is optically dense and thus can serve as an efficient quantum interface. Different micro-ensembles can be individually or collectively accessed in a programmable way through electric control of a set of cross-placed acoustic optical deflectors (AODs) (*13*, *26*), with details described in Materials and Methods. Programmable control of the experimental setup plays an important role for scalable generation of entanglement (*27*).

We use a variation of the Duan-Lukin-Cirac-Zoller (DLCZ) scheme to generate multipartite entanglement between the 2D array of micro-atomic ensembles (*2*). The information in each atom is carried by the hyperfine levels $|g\rangle \equiv |5S_{1/2}, F = 2\rangle$ and $|s\rangle \equiv |5S_{1/2}, F = 1\rangle$ in the ground-state manifold. All the atoms are initially prepared to the state $|g\rangle$ through optical pumping, and this initial state is denoted as $|0\rangle$ for each micro-ensemble. Through the DLCZ scheme, a weak write laser pulse can induce a Raman transition from $|g\rangle$ to $|s\rangle$, scatter a photon to the signal mode in the forward direction with an angle of 2° from the write pulse, and excite a single atom into the corresponding collective spin-wave mode. This state with one collective spin-wave excitation is denoted as $|1_i\rangle$ for the ith micro-ensemble.

We generate multipartite entanglement of the W-state type between micro-ensemble quantum interfaces (*14*, *18*–*22*). For N micro-ensembles, an ideal W state has the form

$$|W_N\rangle = \frac{1}{\sqrt{N}} \sum_{i=1}^{N} e^{i\phi_i} |00\ldots1_i\ldots00\rangle \quad (1)$$

[1]Center for Quantum Information, Institute for Interdisciplinary Information Sciences, Tsinghua University, Beijing 100084, PR China. [2]Department of Physics, University of Michigan, Ann Arbor, MI 48109, USA.
*Corresponding author. Email: lmduan@umich.edu

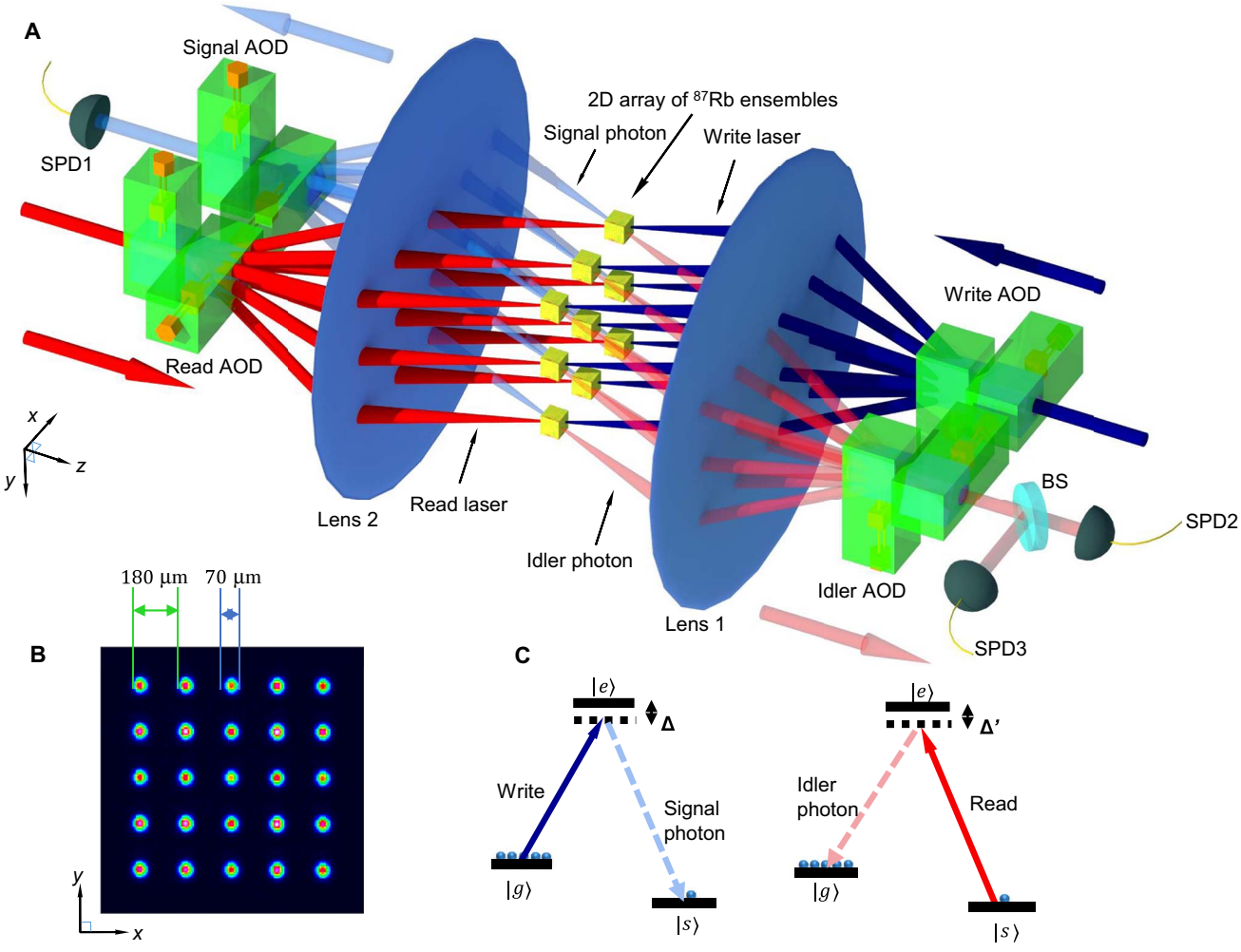

Fig. 1. Experimental setup for generation and verification of multipartite entanglement between a 2D array of atomic quantum interfaces. (**A**) We use a combination of the DLCZ scheme and the programmable AOD multiplexer to generate multipartite entanglement of the W-state type between the atomic spin waves in a 2D array of micro-ensembles. For clarity, we show a 3 × 3 array, albeit we have also entangled 4 × 4 and 5 × 5 ensemble arrays. The write laser beam is split coherently into nine paths to simultaneously excite the 3 × 3 ^{87}Rb ensemble array by the write AOD multiplexer, which contains two orthogonal deflectors placed in the *x* and *y* directions. The lens after the AOD multiplexer focuses the beams and, at the same time, maps different angles of the deflected beams to different positions in a big atomic cloud forming individual micro-ensembles. The scattered signal photon modes are combined phase coherently by lens 2 and the signal AOD de-multiplexer and then coupled into a single-mode fiber with output detected by the single-photon detector (SPD1). To verify multipartite entanglement, we use a programmable AOD multiplexer and de-multiplexer in the paths of the read beam and the idler photon mode to detect the atomic spin waves from different micro-ensembles in several complementary bases. To bound the double excitation probability, the idler photon mode is split by a 50/50 beam splitter (BS) and detected by two single-photon detectors (SPD2 and SPD3) for registration of the three-photon coincidence (together with the SPD1). (**B**) Illustration of the 5 × 5 array from multiplexing of a laser beam at the position of the atomic ensemble. This image is obtained by shining a laser beam into the signal single-mode fiber, which is multiplexed by the signal AOD and captured by a charge-coupled device camera at the position of the atomic ensemble. The separation between adjacent signal modes is 180 μm in both the *x* and *y* directions, and the Gaussian diameter of both the signal and the idler modes is 70 μm. (**C**) Relevant atomic energy levels and their couplings to the write/read laser beams and the signal/idler photon modes, with $|g\rangle \equiv |5S_{1/2}, F = 2\rangle$, $|s\rangle \equiv |5S_{1/2}, F = 1\rangle$, and $|e\rangle \equiv |5P_{1/2}, F' = 2\rangle$. The write (read) laser beam is red-detuned at Δ = 10 MHz (Δ′ = 0), respectively, at the center micro-ensemble.

where, for the *i*th component, we have a stable but adjustable phase factor $e^{i\phi_i}$ and a single collective spin-wave excitation in the *i*th micro-ensemble. The W state corresponds to a type of extremal multipartite entangled state most robust to the particle loss (*18*) and has applications in implementation of quantum information protocols (*2*, *3*, *18*–*22*). To generate the W-state entanglement between *N* micro-ensembles, we split the write laser pulse into *N* beams by the write AODs, as shown in Fig. 1, and coherently combine the signal photon modes from *N* micro-ensembles by the signal AODs with equal weight into a single direction, which is coupled to a single-mode fiber for detection. When we register a signal photon by the detector, this photon is equally likely to come from each micro-ensemble, which has an atomic excitation in the corresponding spin-wave mode. The final state of *N* micro-ensembles is described by the W state (*1*) in the ideal case as the AODs maintain coherence between different optical superposition paths.

Verification of multipartite entanglement

The experimentally prepared state differs from the ideal form (*1*) from contribution of several noises and imperfections. First, there is a small but nonzero probability to generate double or higher-order excitations of the photon–spin-wave pair. Second, the spin-wave mode could be in the vacuum state when we registered a photon due to the imperfect

atom-photon correlation or the excitation loss in the atomic memory. Finally, even with exactly one spin-wave excitation, it may not distribute equally or perfectly coherently among N micro-ensembles. The experimental state ρ_e can be expressed as

$$\rho_e = p_0\rho_0 + p_1\rho_1 + p_2\rho_2 \quad (2)$$

where p_0, p_1, p_2 and ρ_0, ρ_1, ρ_2, denote the population and the corresponding density matrix with zero, one, and double excitations in the spin-wave modes, respectively. The state fidelity is defined as $F = \langle W_N|\rho_e|W_N\rangle = p_1\langle W_N|\rho_1|W_N\rangle$. In Eq. 2, we have cut the expansion to the second-order excitations by neglecting tiny higher-order terms. If we assume a Poisson distribution for the number of excitations (which is the case for a parametric light-atom interaction under weak pumping), we can estimate the contribution of the higher-order excitations from the measured p_2/p_1. Their influence turns out to be negligible to all our subsequent results (see section S2).

To verify multipartite quantum entanglement between N quantum interfaces, we use entanglement witness to lower bound the entanglement depth k ($k \leq N$) (*28*), which means that the state ρ_e has at least k-partite genuine quantum entanglement (*29*). An entanglement witness appropriate for the W-type entangled state is given by $\mathcal{W}_k = \alpha_k P_0 + \beta_k P_1 + \gamma_k P_2 - |W_N\rangle\langle W_N|$ (*29*), where P_n (n = 0, 1, and 2) denote the projectors onto the subspace with n excitations in the spin-wave modes and the parameters α_k, β_k, $\gamma_k \geq 0$ are numerically optimized (see section S1) such that for any state ρ_a with entanglement depth less than k, the witness is non-negative, that is, $\mathrm{tr}[\mathcal{W}_k\rho_a] = \alpha_k p_0 + \beta_k p_1 + \gamma_k p_2 - F \geq 0$. Therefore, $\mathrm{tr}[\mathcal{W}_k\rho_e] < 0$ serves as a sufficient condition to verify that we have at least k-partite genuine entanglement among the N quantum interfaces. Note that this witness does not require $p_0 + p_1 + p_2 = 1$, so it also applies in the case with $p_0 + p_1 + p_2 < 1$ when we consider small higher-order excitations, although the corrections turn out to be negligible for all our subsequent results (see the Supplementary Materials).

To bound the entanglement depth, we experimentally measure the fidelity F and the population p_0, p_1, p_2. The detailed measurement procedure is explained in section S2. The spin-wave excitation in each quantum interface is retrieved to the idler photon for detection by a read laser beam. Our measurement is directly on the state of the retrieved photon, which can be represented by a form similar to Eq. 2 for the spin-wave modes. Because of the limited retrieval efficiency, detector inefficiency, and the associated photon loss, the detected idler photon modes have much larger vacuum components, and their corresponding parameters are denoted as F' and p'_0, p'_1, p'_2. Because this retrieval process is a local operation, the entanglement in the retrieved photonic modes provides a lower bound to the entanglement in the collective spin-wave modes in the atomic ensembles (*14*).

The fidelity F' and the populations p'_0, p'_1, p'_2 of the idler photon are determined in the following way. We first measure the double excitation probability p'_2 from the photon intensity correlation of the two single-photon detectors in the idler modes, conditioned on a photon click in the signal mode. Then, p'_1, p'_0, and F' are measured by programming the four sets (write, signal, read, and idler) of AODs in different configurations, as shown in Fig. 2 (see details in section S2 and figs. S1 to S4). When we measure the population p'_1, the idler AOD successively picks up the output photon mode of each individual micro-ensemble for detection; as for the fidelity F', the idler AOD coherently combines the output idler modes from the N micro-ensembles with equal weight to the single-mode fiber for detection, which gives an effective projection to the state $|W_N\rangle$. Note that the fidelity measurement is sensitive to the relative phase information between different idler photon modes because these modes interfere at the AODs through the coherent combination. After F' and p'_0, p'_1, p'_2 are measured, we calibrate the retrieval efficiency for each micro-ensemble and finally derive the fidelity F and populations p_0, p_1, p_2 of the spin-wave modes from the measured idler

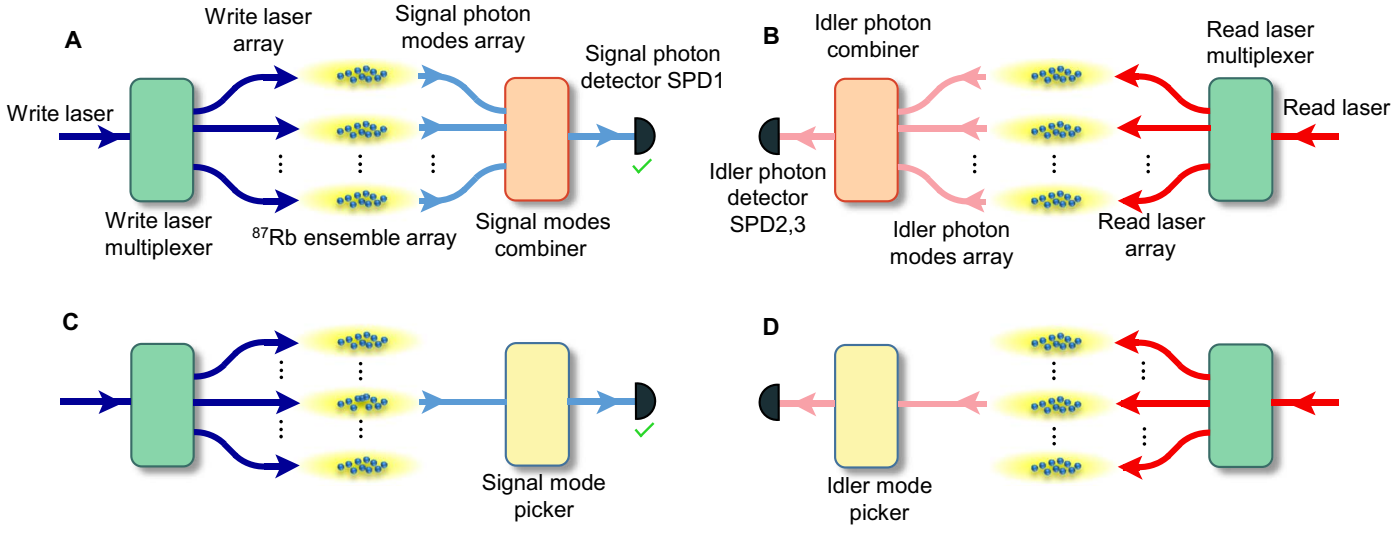

Fig. 2. Programmable coupling configurations for entanglement generation and verification. (**A**) The coupling configuration to generate multipartite entanglement, where the write AODs split the optical paths and the signal AODs coherently combine the paths. (**B**) The detection configuration for the measurement of fidelity, where the read AODs deliver the read beams to all the micro-ensembles to transfer the atomic spin-wave excitations to idler photons, and the idler AODs combine coherently the idler modes from different ensembles with equal weight for detection in the superposition basis. (**C** and **D**) The write and the read AODs in (C) and (D) are configured in the same way as those in (A) and (B), but the signal and the idler AODs are programmed to successively detect the signal/idler photon from each individual micro-ensemble. The configurations (C) and (D) combined are used to calibrate the retrieval efficiency for each micro-ensemble, and the configurations (A) and (D) combined are used to detect the excitation population in each ensemble after the W-state preparation (see section S2 for details).

A

p_0'	p_1'	p_2'	F'	W_8'
$95.8 \pm 0.1\%$	$4.2 \pm 0.1\%$	$2.8 \pm 0.9 \times 10^{-5}$	$4.01 \pm 0.03\%$	-0.0032 ± 0.0012

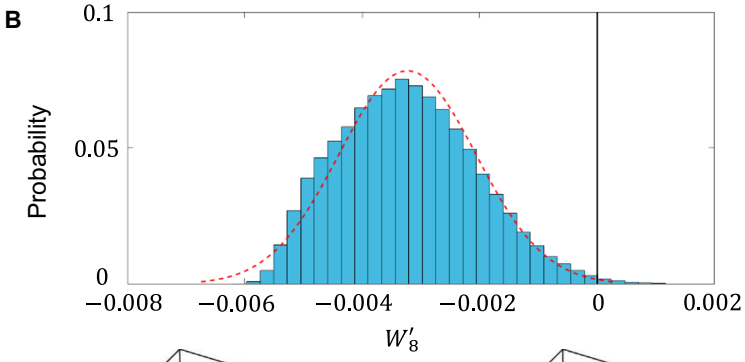

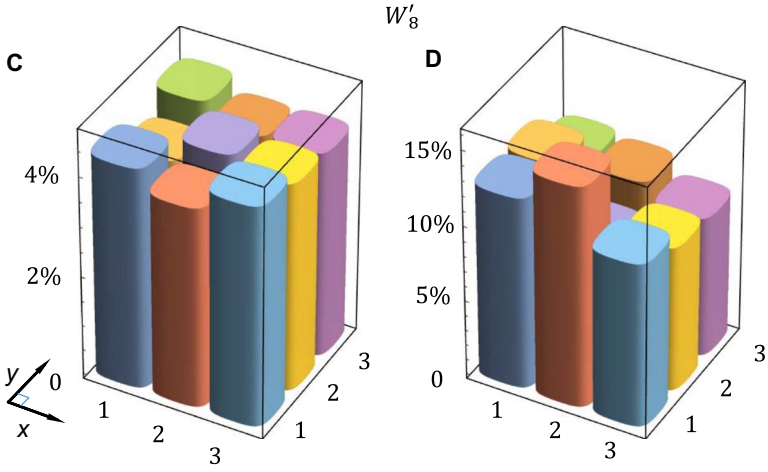

E

p_0	p_1	p_2	F	W_9
$2.0^{+2.5}_{-2.0}\%$	$96.5^{+2.1}_{-2.5}\%$	$1.5 \pm 0.5\%$	$92.2 \pm 1.6\%$	-0.053 ± 0.015

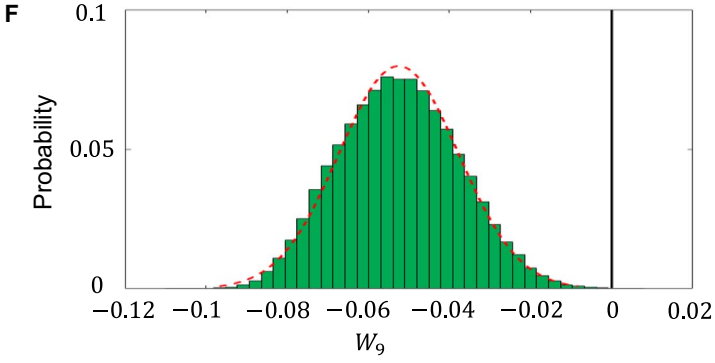

Fig. 3. Entanglement verification for the 3 × 3 array of atomic ensembles. (**A**) The measured values, together with the 68% confidence intervals (corresponding to the region within 1 SD if the distribution is Gaussian), for the population p_0', p_1', p_2', the fidelity F', and the entanglement witness W_8' for the idler photon modes that are directly measured. The entanglement in the retrieved idler photon modes provides a lower bound to the entanglement in the collective spin-wave modes in different atomic ensembles. The optimized parameters in the witness W_8' are given by $\alpha_8' = 2.259 \times 10^{-3}$, $\beta_8' = 0.7898$, and $\gamma_8' = 49.13$. (**B**) The distribution of entanglement witness W_8', where $W_8' < 0$ implies eight-partite genuine entanglement. The probability with $W_8' < 0$ is 99.5% from this measurement. (**C**) The measured retrieval efficiency for each of the 3 × 3 atomic ensemble arrays. (**D**) The measured spin-wave excitation population in each of the 3 × 3 atomic ensemble arrays after the W-state preparation. (**E**) The measured values, together with the 68% confidence intervals for the population p_0, p_1, p_2, the fidelity F, and the entanglement witness W_9 for the collective spin-wave modes in different atomic ensembles after correction of the retrieval efficiency through the above measurements. The optimized parameters in the witness W_9 are given by $\alpha_9 = 0.369$, $\beta_9 = 0.889$, and $\gamma_9 = 0.268$. (**F**) The distribution of entanglement witness W_9, where $W_9 < 0$ implies nine-partite genuine entanglement. The probability with $W_9 < 0$ is 99.98% from this measurement.

photon statistics (*30*). The detailed conversion procedure is described in section S2.

We have performed the entanglement preparation and verification experiments with 3 × 3, 4 × 4, and 5 × 5 arrays of micro-ensembles. For nine individually addressable micro-ensembles, the results are shown in Fig. 3. We present the parameters for the idler photon state in Fig. 3A, and the probability to have eight-partite entanglement is 99.5% for the photon state. After conversion with the calibrated retrieval efficiency, we find that the state of the atomic micro-ensembles has a high fidelity of $F = (92.2 \pm 1.6)\%$ to be in the nine-partite W state. In Fig. 3D, we show the distribution of the entanglement witness $W_9 = \mathrm{tr}[\mathcal{W}_9\rho_e]$ from the experimental data. From this distribution, we conclude with a confidence level of 99.98% that we have generated genuine nine-partite quantum entanglement among the nine atomic ensembles.

In Figs. 4 and 5, we show the experimental results for 16 and 25 micro-ensembles. In these cases, the fidelity is not high enough to prove that all of them are genuinely entangled. The calibrated fidelities F for the atomic states are $(84.9 \pm 1.7)\%$ and $(83.9 \pm 1.4)\%$, respectively. With more ensembles, it becomes harder to maintain the uniformity in the optical depth and the laser excitation probability for each ensemble, which causes the fidelity to decay. However, we can still use the entanglement witness to demonstrate a high entanglement depth. As shown in Figs. 4 and 5, for 16 ensembles, we have confirmed 11-partite entanglement in the retrieved idler photon modes with a confidence level of 99.7% and 14-partite entanglement between the spin-wave modes in the 16 micro-ensembles with a confidence level of 99.997% after correction with the calibrated retrieval efficiency; for 25 ensembles, we have confirmed 17-partite entanglement in the retrieved photonic modes with a confidence level of 98.4% and 22-partite entanglement between the 25 micro-ensembles with a confidence level of 96.5%.

DISCUSSION

Our experimental preparation of multipartite entanglement in a record-high number of individually addressable quantum interfaces represents a significant milestone in quantum state engineering.

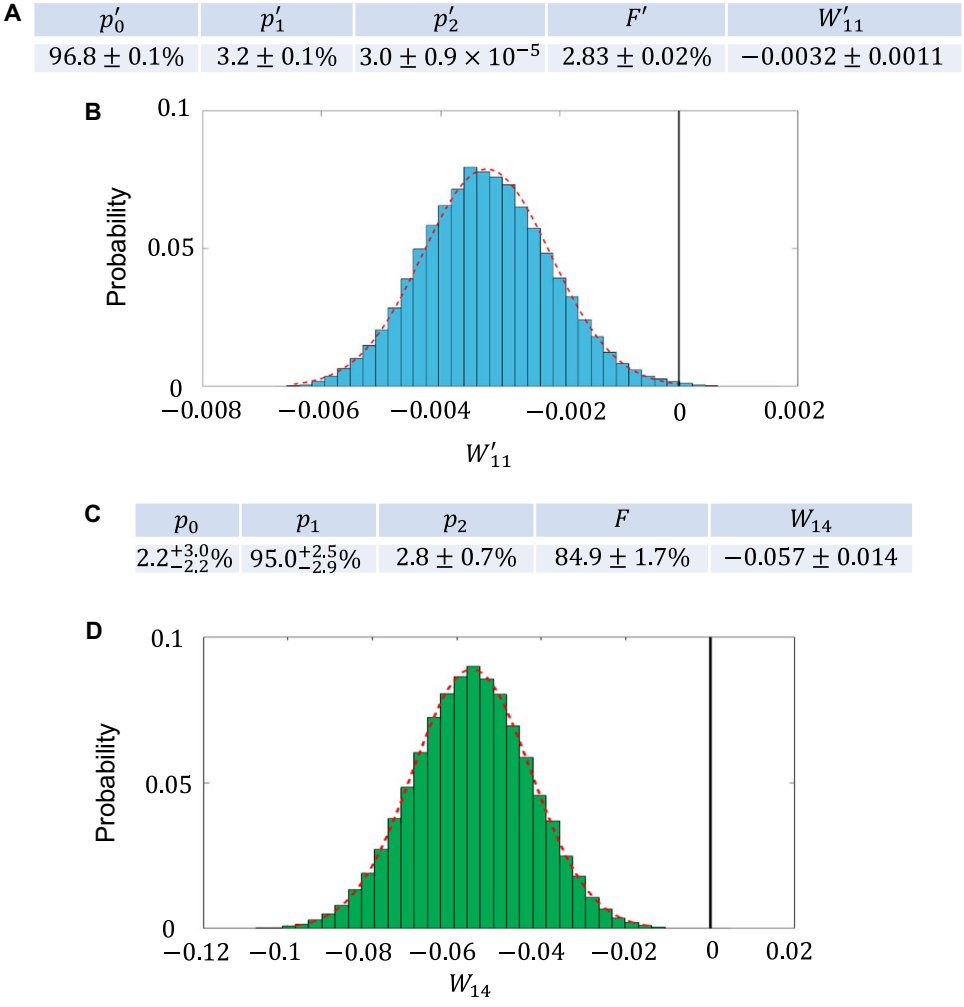

Fig. 4. Entanglement verification for the 4 × 4 array of atomic ensembles. (**A**) The measured values, together with the 68% confidence intervals, for the population p_0', p_1', p_2', the fidelity F', and the entanglement witness W_{11}' for the directly measured idler photon modes retrieved from the 4 × 4 atomic ensemble array. The optimized parameters in the witness W_{11}' are given by $\alpha_{11}' = 3.152 \times 10^{-3}$, $\beta_{11}' = 0.6370$, and $\gamma_{11}' = 58.14$. (**B**) The distribution of entanglement witness W_{11}' for the 4 × 4 idler photon modes. The probability with $W_{11}' < 0$ is 99.7% from these measurements. (**C**) The measured values, together with the 68% confidence intervals, for the population p_0, p_1, p_2, the fidelity F, and the entanglement witness W_{14}, for the 4 × 4 atomic ensemble array after correction of the retrieval efficiency. The optimized parameters in the witness W_{14} are given by $\alpha_{14} = 0.635$, $\beta_{14} = 0.813$, and $\gamma_{14} = 0.240$. (**D**) The distribution of entanglement witness W_{14} for the 4 × 4 case. The probability with $W_{14} < 0$ is 99.997% from these measurements.

A

p_0'	p_1'	p_2'	F'	W_{17}'
$96.3 \pm 0.1\%$	$3.7 \pm 0.1\%$	$4.4 \pm 1.1 \times 10^{-5}$	$3.22 \pm 0.02\%$	-0.0028 ± 0.0013

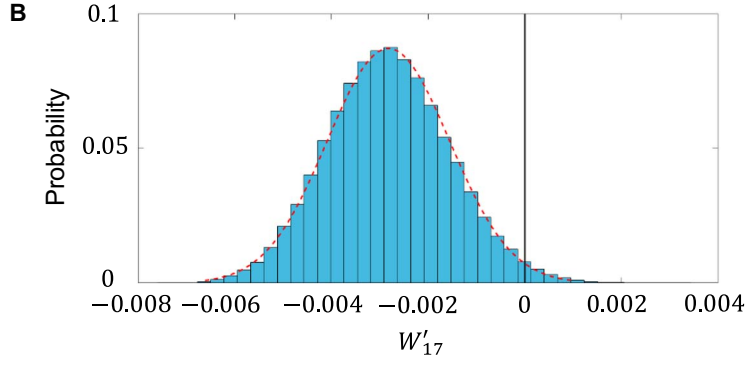

C

p_0	p_1	p_2	F	W_{22}
$2.4^{+3.0}_{-2.4}\%$	$94.6^{+2.5}_{-2.9}\%$	$3.0 \pm 0.7\%$	$83.9 \pm 1.4\%$	-0.024 ± 0.013

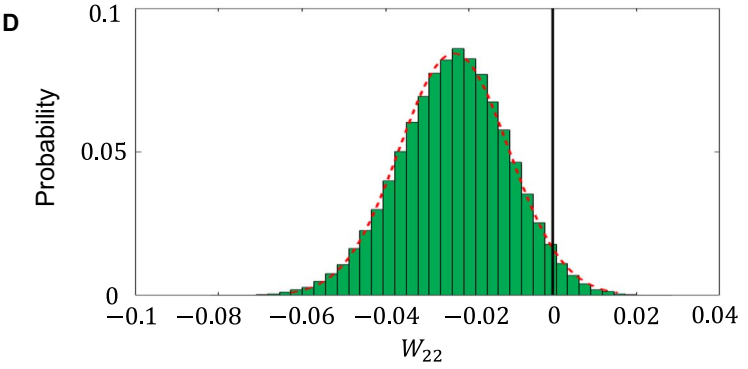

Fig. 5. Entanglement verification for the 5 × 5 array of atomic ensembles. (**A**) The measured values, together with the 68% confidence intervals, for the population p_0', p_1', p_2', the fidelity F', and the entanglement witness W_{17}' for the directly measured idler photon modes retrieved from the 5 × 5 atomic ensemble array. The optimized parameters in the witness W_{17}' are given by $\alpha_{17}' = 3.317 \times 10^{-3}$, $\beta_{17}' = 0.6516$, and $\gamma_{17}' = 53.65$. (**B**) The distribution of entanglement witness W_{17}' for the 5 × 5 idler photon modes. The probability with $W_{17}' < 0$ is 98.4% from these measurements. (**C**) The measured values, together with the 68% confidence intervals, for the population p_0, p_1, p_2, the fidelity F, and the entanglement witness W_{22} for the 5 × 5 atomic ensemble array after correction of the retrieval efficiency. The optimized parameters in the witness W_{22} are given by $\alpha_{22} = 0.550$, $\beta_{22} = 0.840$, and $\gamma_{22} = 0.244$. (**D**) The distribution of entanglement witness W_{22} for the 5 × 5 case. The probability with $W_{22} < 0$ is 96.5% from these measurements.

Through programming of AODs to control intrinsically stable optical interference paths, the entanglement preparation and verification techniques developed in this experiment are fully scalable to a larger number of quantum interfaces. It is feasible to use AODs to program and direct the focused laser beams to hundreds of micro-ensembles (*26*). The number of entangled ensembles in our current experiment is basically limited by the size of the whole atomic cloud and the available optical depth. With the use of double magneto-optical traps (MOTs) for more efficient atom loading, we can significantly increase the size of the atomic cloud, the optical depth, and the retrieval efficiency for the stored photons. In that case, we should be able to obtain hundreds of micro-ensembles entangled by the same control setup and entanglement verification techniques reported in this experiment. Generation of multipartite entanglement between many individually addressable quantum interfaces demonstrates an important step toward the realization of quantum networks (*2*, *3*), long-distance quantum communication (*2*, *4*, *5*), and multipartite quantum information processing (*3*, *14*, *18*, *19*).

Note added. After posting this work on arXiv (arXiv:1707.09701), we became aware of related independent works by Zarkeshian *et al.* (*31*) and Fröwis *et al.* (*32*), which report generation of multiparticle W-state entanglement in solid-state ensembles. Compared with those experiments, we realized multipartite entanglement between spatially separated micro-ensembles of neutral atoms, which are individually accessible by focused laser beams with programmable control of the AODs. We thank C. Simon for bringing the work of Zarkeshian *et al.* (*31*) and Fröwis *et al.* (*32*) to our attention.

MATERIALS AND METHODS

Experimental methods

A ^{87}Rb atomic cloud was loaded into a MOT. For cooling and trapping of the atoms in the MOT, a strong cooling beam, red-detuned to the D2 cycling transition $|g\rangle \equiv |5S_{1/2}, F = 2\rangle \rightarrow |5P_{3/2}, F = 3\rangle$ by 12 MHz, was used. The repumping laser, resonant to the $|s\rangle \equiv |5S_{1/2}, F = 1\rangle \rightarrow |5P_{3/2}, F = 2\rangle$ transition, pumped back atoms that fell out of the cooling transition. The temperature of the atoms was about 300 μK in the MOT. The atoms were then further cooled by polarization gradient cooling (PGC) for 1 ms. The PGC was implemented by increasing the red-detuning of

the cooling laser to 60 MHz and by reducing the intensity to half of the value at the MOT loading stage. At the same time, the repumping laser intensity was decreased to 0.5% of the value at the loading phase, and the magnetic gradient coil was shut off. The temperature was reduced to about 30 μK after this process, and the size of the MOT remained almost the same. After the PGC, some atoms were scattered to the $|s\rangle$ state, and we used a 100-μs repumping pulse to pump all the atoms back to $|g\rangle$. During the storage, the ambient magnetic field was not compensated; thus, the retrieval efficiency of the collective spin-wave excitation underwent Larmor precession. In our case, the Larmor period was 5.8 μs. The time interval between the read and the write pulses was set to this Larmor period to achieve the highest retrieval efficiency for the idler photon.

The experimental sequence began with a write pulse of 100 ns long, which was split by the write AODs to N paths to excite the 2D array of atomic ensembles. If no signal photon was detected, a clearance pulse identical to the read pulse pumped the atoms back to $|g\rangle$. The write-clearance sequence was repeated until a signal photon was detected. Upon detection of the signal photon, the corresponding collective spin-wave excitation was stored in the atomic ensemble for a controllable period of time and then retrieved by a read pulse to a photon in the idler mode. The conditional control of write/read pulses was implemented by a field-programmable gate array (FPGA). The signal or idler photons collected by the single-mode optical fiber were directed to a single-photon counting module. The photon countings and their coincidence were registered through the FPGA.

Control of AODs

The radio-frequency (RF) signal was generated by two 4-channel arbitrary waveform generators (AWGs; Tektronix 5014C). One of the AWG supplied the RF for write, read, signal, and idler AODs (AA DTSXY-400) in the x direction, and the other supplied the RF for the AODs in the y direction. The outputs of the AWG channels were amplified by a 2-W RF amplifier (Mini-Circuits, ZHL-1-2W) to drive the AODs.

The nonlinearity in the amplifier and the AODs could induce other unwanted frequency components, which cause imperfections in the mode multiplexing and de-multiplexing. By carefully tuning the relative phases in read, signal, and idler AODs, as discussed by Endres *et al.* (*33*), we can attenuate the influence from these unwanted frequency components by an extinction ratio of about 120 dB, which becomes negligible for our experiment.

Although the AODs split the optical paths into many different branches, the relative optical phases between different branches were intrinsically stable as different optical paths in our experiment went through the same optics elements. This is an important advantage that eliminates the need for complicated active phase stabilization for many optical interferometer loops in our experiment. The relative phases between different superposition paths were adjusted in experiments by controlling the phases of different RF components that drove the write AODs.

SUPPLEMENTARY MATERIALS

Supplementary material for this article is available at http://advances.sciencemag.org/cgi/content/full/4/4/eaar3931/DC1

section S1. Entanglement witness for W-type states

section S2. Experimental measurement of the entanglement witness

section S3. Discussion of the experimental noise

fig. S1. Coupling configuration for the measurement of the retrieval efficiency of each micro-ensemble.

fig. S2. Coupling configuration for the measurement of the excitation population of each micro-ensemble.

fig. S3. Coupling configuration for the measurement of the W-state fidelity.

fig. S4. Measurement of the three-photon correlation and the double excitation probability.

REFERENCES AND NOTES

1. K. Hammerer, A. S. Sørensen, E. S. Polzik, Quantum interface between light and atomic ensembles. *Rev. Mod. Phys.* **82**, 1041–1093 (2010).
2. L.-M. Duan, M. D. Lukin, J. I. Cirac, P. Zoller, Long-distance quantum communication with atomic ensembles and linear optics. *Nature* **414**, 413–418 (2001).
3. H. J. Kimble, The quantum internet. *Nature* **453**, 1023–1030 (2008).
4. H.-J. Briegel, W. Dür, J. I. Cirac, P. Zoller, Quantum repeaters: The role of imperfect local operations in quantum communication. *Phys. Rev. Lett.* **81**, 5932–5935 (1998).
5. N. Sangouard, C. Simon, H. de Riedmatten, N. Gisin, Quantum repeaters based on atomic ensembles and linear optics. *Rev. Mod. Phys.* **83**, 33–80 (2011).
6. O. A. Collins, S. D. Jenkins, A. Kuzmich, T. A. B. Kennedy, Multiplexed memory-insensitive quantum repeaters. *Phys. Rev. Lett.* **98**, 060502 (2007).
7. C.-W. Chou, H. de Riedmatten, D. Felinto, S. V. Polyakov, S. J. van Enk, H. J. Kimble, Measurement-induced entanglement for excitation stored in remote atomic ensembles. *Nature* **438**, 828–832 (2005).
8. T. Chanelière, D. N. Matsukevich, S. D. Jenkins, S.-Y. Lan, T. A. B. Kennedy, A. Kuzmich, Storage and retrieval of single photons transmitted between remote quantum memories. *Nature* **438**, 833–836 (2005).
9. M. D. Eisaman, A. André, F. Massou, M. Fleischhauer, A. S. Zibrov, M. D. Lukin, Electromagnetically induced transparency with tunable single-photon pulses. *Nature* **438**, 837–841 (2005).
10. B. Julsgaard, J. Sherson, J. I. Cirac, J. Fiurášek, E. S. Polzik, Experimental demonstration of quantum memory for light. *Nature* **432**, 482–486 (2004).
11. J. Simon, H. Tanji, S. Ghosh, V. Vuletić, Single-photon bus connecting spin-wave quantum memories. *Nat. Phys.* **3**, 765–769 (2007).
12. H. de Riedmatten, M. Afzelius, M. U. Staudt, C. Simon, N. Gisin, A solid-state light–matter interface at the single-photon level. *Nature* **456**, 773–777 (2008).
13. S.-Y. Lan, A. G. Radnaev, O. A. Collins, D. N. Matsukevich, T. A. B. Kennedy, A. Kuzmich, A multiplexed quantum memory. *Opt. Express* **17**, 13639–13645 (2009).
14. K. S. Choi, A. Goban, S. B. Papp, S. J. van Enk, H. J. Kimble, Entanglement of spin waves among four quantum memories. *Nature* **468**, 412–416 (2010).
15. E. Saglamyurek, N. Sinclair, J. Jin, J. A. Slater, D. Oblak, F. Bussières, M. George, R. Ricken, W. Sohler, W. Tittel, Broadband waveguide quantum memory for entangled photons. *Nature* **469**, 512–515 (2011).
16. S.-J. Yang, X.-J. Wang, X.-H. Bao, J.-W. Pan, An efficient quantum light–matter interface with sub-second lifetime. *Nat. Photonics* **10**, 381–384 (2016).
17. C.-W. Chou, J. Laurat, H. Deng, K. S. Choi, H. de Riedmatten, D. Felinto, H. J. Kimble, Functional quantum nodes for entanglement distribution over scalable quantum networks. *Science* **316**, 1316–1320 (2007).
18. W. Dür, G. Vidal, J. I. Cirac, Three qubits can be entangled in two inequivalent ways. *Phys. Rev. A* **62**, 062314 (2000).
19. J. Joo, Y.-J. Park, S. Oh, J. Kim, Quantum teleportation via a *W* state. *New J. Phys.* **5**, 136 (2003).
20. H. Häffner, W. Hänsel, C. F. Roos, J. Benhelm, D. Chek-al-kar, M. Chwalla, T. Körber, U. D. Rapol, M. Riebe, P. O. Schmidt, C. Becher, O. Gühne, W. Dür, R. Blatt, Scalable multiparticle entanglement of trapped ions. *Nature* **438**, 643–646 (2005).
21. F. Haas, J. Volz, R. Gehr, J. Reichel, J. Estève, Entangled states of more than 40 atoms in an optical fiber cavity. *Science* **344**, 180–183 (2014).
22. R. McConnell, H. Zhang, J. Z. Hu, S. Ćuk, V. Vuletić, Entanglement with negative Wigner function of almost 3,000 atoms heralded by one photon. *Nature* **519**, 439–442 (2015).
23. T. Monz, P. Schindler, J. T. Barreiro, M. Chwalla, D. Nigg, W. A. Coish, M. Harlander, W. Hänsel, M. Hennrich, R. Blatt, 14-qubit entanglement: Creation and coherence. *Phys. Rev. Lett.* **106**, 130506 (2011).
24. X.-L. Wang, L.-K. Chen, W. Li, H.-L. Huang, C. Liu, C. Chen, Y.-H. Luo, Z.-E. Su, D. Wu, Z.-D. Li, H. Lu, Y. Hu, X. Jiang, C.-Z. Peng, L. Li, N.-L. Liu, Y.-A. Chen, C.-Y. Lu, J.-W. Pan, Experimental ten-photon entanglement. *Phys. Rev. Lett.* **117**, 210502 (2016).
25. C. Song, K. Xu, W.-X. Liu, C.-p. Yang, S.-B. Zheng, H. Deng, Q.-W. Xie, K.-Q. Huang, Q.-J. Guo, L.-B. Zhang, P.-F. Zhang, D. Xu, D.-N. Zheng, X.-B. Zhu, H. Wang, Y.-A. Chen, C.-Y. Lu, S.-Y. Han, J.-W. Pan, 10-qubit entanglement and parallel logic operations with a superconducting circuit. *Phys. Rev. Lett.* **119**, 180511 (2017).
26. Y.-F. Pu, N. Jiang, W. Chang, H.-X. Yang, C. Li, L.-M. Duan, Experimental realization of a multiplexed quantum memory with 225 individually accessible memory cells. *Nat. Commun.* **8**, 15359 (2017).

27. S. Debnath, N. M. Linke, C. Figgatt, K. A. Landsman, K. Wright, C. Monroe, Demonstration of a small programmable quantum computer with atomic qubits. *Nature* **536**, 63–66 (2016).
28. A. S. Sørensen, K. Mølmer, Entanglement and extreme spin squeezing. *Phys. Rev. Lett.* **86**, 4431–4434 (2001).
29. O. Gühne, G. Tóth, Entanglement detection. *Phys. Rep.* **474**, 1–75 (2009).
30. C. W. Chou, S. V. Polyakov, A. Kuzmich, H. J. Kimble, Single-photon generation from stored excitation in an atomic ensemble. *Phys. Rev. Lett.* **92**, 213601 (2004).
31. P. Zarkeshian, C. Deshmukh, N. Sinclair, S. K. Goyal, G. H. Aguilar, P. Lefebvre, M. Grimau Puigibert, V. B. Verma, F. Marsili, M. D. Shaw, S. W. Nam, K. Heshami, D. Oblak, W. Tittel, C. Simon, Entanglement between more than two hundred macroscopic atomic ensembles in a solid. *Nat. Commun.* **8**, 906 (2017).
32. F. Fröwis, P. C. Strassmann, A. Tiranov, C. Gut, J. Lavoie, N. Brunner, F. Bussières, M. Afzelius, N. Gisin, Experimental certification of millions of genuinely entangled atoms in a solid. *Nat. Commun.* **8**, 907 (2017).
33. M. Endres, H. Bernien, A. Keesling, H. Levine, E. R. Anschuetz, A. Krajenbrink, C. Senko, V. Vuletic, M. Greiner, M. D. Lukin, Atom-by-atom assembly of defect-free one-dimensional cold atom arrays. *Science* **354**, 1024–1027 (2016).

Acknowledgments: We thank A. Kuzmich and Y.-M. Liu for discussions. **Funding:** This work was supported by the Ministry of Education and the National key Research and Development Program of China. L.D. acknowledges support from the Army Research Laboratory Center for Distributed Quantum Information program. **Author contributions:** L.D. conceived the experiment and supervised the project. Y.P., N.J., W.C., C.L., and S.Z. carried out the experiment. Y.W. optimized the entanglement witness. L.D., Y.P., and Y.W. wrote the manuscript. **Competing interests:** The authors declare that they have no competing interests. **Data and materials availability:** All data needed to evaluate the conclusions in the paper are present in the paper and/or the Supplementary Materials. Additional data related to this paper may be requested from the authors.

Submitted 2 November 2017
Accepted 1 March 2018
Published 20 April 2018
10.1126/sciadv.aar3931

Citation: Y. Pu, Y. Wu, N. Jiang, W. Chang, C. Li, S. Zhang, L. Duan, Experimental entanglement of 25 individually accessible atomic quantum interfaces. *Sci. Adv.* **4**, eaar3931 (2018).

Experimental entanglement of 25 individually accessible atomic quantum interfaces

Yunfei Pu, Yukai Wu, Nan Jiang, Wei Chang, Chang Li, Sheng Zhang and Luming Duan

Sci Adv **4** (4), eaar3931.
DOI: 10.1126/sciadv.aar3931